Effect of Localized Damages on the Free Vibration Analysis of Civil Structures by Component-Wise Approach

Effect of Localized Damages on the Free Vibration Analysis of Civil Structures by Component-Wise Approach.

T. Cavallo*, A. Pagani†E. Zappino‡and E. Carrera§

Submitted to: Journal of Structural Engineering (ASCE)

*Research assistant
MUL^2, Department of Mechanical and Aerospace Engineering, Politecnico di Torino
Corso Duca degli Abruzzi 24, 10129 Torino, Italy.
†Professor assistant
MUL^2, Department of Mechanical and Aerospace Engineering, Politecnico di Torino
Corso Duca degli Abruzzi 24, 10129 Torino, Italy
E-mail: alfonso.pagani@polito.it
‡Professor assistant
MUL^2, Department of Mechanical and Aerospace Engineering, Politecnico di Torino
Corso Duca degli Abruzzi 24, 10129 Torino, Italy
E-mail: enrico.zappino@polito.it
§Professor, author for correspondence
MUL^2, Department of Mechanical and Aerospace Engineering, Politecnico di Torino
Corso Duca degli Abruzzi 24, 10129 Torino, Italy
E-mail: erasmo.carrera@polito.it

Abstract

Refined one-dimensional, 1D, models are used to carry out free vibration analysis of civil engineering structures affected by local damages. The Carrera Unified Formulation (CUF) provides higher-order structural models to be formulated in a compact and, eventually, hierarchical manner. In the domain of the CUF, refined $1D$ *models characterized by three-dimensional capabilities can be realized by using various function expansions of the generalized displacement field over the cross-section. Recently, a component-wise (CW) approach was introduced by employing CUF. CW gives a detailed physical description of multi-component structures since each component can be modeled with its geometrical and mechanical characteristics; namely, no reference surfaces and axes as well as no homogenization techniques, are employed. In the present work, combinations of quadratic Lagrange elements are used to describe the beam theory kinematics. This approach allows to analyze with high accuracy complex civil structures, such as truss structures, industrial buildings and a multi-floor building. In this context, damage scenarios are introduced with no loss of accuracy in the mathematical formulation by deteriorating the single component of the structure. Effect of damages are, thus, evaluated by free vibration analyses.*

1 Introduction

Stiffness, and consequently, the modal characteristics of structures are widely affected by the state of health of each structural component. The earthquakes and common daily movements carry out an important role for the structural integrity. Considerable theoretical and experimental advantages have been made in structural civil control. In particular, over the last 30 years, various damage monitoring system have been introduced to allow engineers to control the significant displacements of the structure, especially during catastrophic events. In the early 1990's, Wu et al. 1992 have introduced conceptual models for the sensor locations, signal transmission, and central processing of information for simple structure systems. Doebling and Farrar 1997 and also Pirner and Fisher 1997, have shown premise for identification of system behaviour and critical parameter benchmarking using laboratory and field experimentation with frame structures and bridges. In the same years, Kiremidjian et al. 1997, have proposed various techniques used for the monitoring of civil infrastructures.

For the past thirty years, the skills in various communication technologies, e.g. wireless communication and global positioning system (GPS), coupled to sensors with higher tolerance and precision, and computational unit with increased power, provided the tools for a potentially new solution to the civil monitoring problem. Different strategies and systems can be used for monitoring the civil structures and identifying various critical damage level without the use of experimental tests. The damage affects the vibration characteristics of the structure, and this has been exploited in many works. The vibration response of a carbon-fiber-reinforced polymer damaged beam was analyzed by Capozucca 2014. Pérez et al. 2014 have conducted an extensive experimental activity to investigate the effects of damages on the vibrations of composite laminates. Wang et al. 2014 have proposed a new approach based on the finite element method (FEM) for damage detection and diagnosis of parts of the engine, wind turbine blades, concerning dynamic analysis and the effects on the modal shape curvatures. Labib and Featherston 2014 have used the dynamic stiffness method to analyze the free vibration of frames including multiple cracks by modeling the crack with rotational springs. Nguyen 2014 adopted three-dimensional (3-D) beam elements to determine the mode shapes for damage detection of broken beam with a rectangular cross-section. Yu et al. 2002 introduced a method where each blade was modelled as a beam based on geometrically nonlinear 3D elasticity theory and by applying variational asymptotic beam sectional (VABS) analysis. The same method has been used recently by Pollayi and Yu 2014 to investigate the effects of the first damage mode via matrix micro-cracking on the mechanical behavior in the helicopter rotor and the wind turbine blades. Recently, Zhang et al. 2016 used a graphical technique to evaluate the position and the hardness of delamination in composite structures by analyzing the frequency alterations introduced by damages.

For damaged structures, the main step is to create a database where the information about natural frequencies and mode shapes for a large spectrum of damage cases must be included. Various mathematical modeling and modal analysis can be used to create databases for the structure under consideration. This aspect, although being rather questionable due to the lack of repeatability of the experiments even under very well controlled conditions, is out of the scope of this paper, and further details can be found in the work of Pérez et al. 2014. In the case of damaged structures, computational models should be able to provide enhanced accuracy in terms of displacements and stress fields. Accuracy is a limit for the classical beam theories based on the one-dimensional approximations. The first 1D theories can be referred to as the Euler Bernoulli Beam Model (EBBM), Euler 1744, and the Timoshenko Beam Model (TBM). The scientific community has continuously worked to develop 1D models able to enhance the classical theories and to extend these models to any geometry or boundary condition and mechanical complexity. The use of correction factors is one of the standard methods adopted to remove some limitations, as in the books of Sokolnikoff 1956 and Timoshenko and Goodier 1970. For example, El Fatmi 2007a introduced a warping function φ to improve the description of the normal and shear stresses over the cross-section. Schardt 1989 developed generalized beam theories (GBT), which were then widely used by Silvestre and Camotim 2002 for the analysis of thin-walled structures. Other refined beam models can be found in work by Kapania and Raciti 1989a and Kapania and Raciti 1989b, which focused on bending, vibration, wave propagations, buckling, and post-buckling. In 1992 a new approach based on an asymptotic solution in which a characteristic parameter (e.g., the cross-section thickness of a beam) is utilized to build an asymptotic series by Berdichevsky et al. 1992 and Carrera et al. 2015b.

The present work exploits the Carrera Unified Formulation (CUF) for higher-order 1D models, see Carrera et al. 2011 and Carrera et al. 2014a. In the present 1D models, the displacement field above the cross-section is modeled through expansion functions for which the order is a free parameter of the analysis. CUF first appeared in the work of Carrera 1995 where it was used to derive a class of 2D theories using a compact formulation. In the works of Carrera 2002 and Carrera 2003, CUF was applied to multi-layered, anisotropic,

composite plates and shells. A few years later, Carrera and Giunta 2010a adopted the CUF for the analysis of 1D models. The most recent extension of the CUF models is the so-called Component-Wise (CW) approach, according to a complex structure can be modeled by joining different components via 1D refined approximation theories. Carrera et al. 2013b, Carrera et al. 2013a, Carrera et al. 2014b and Carrera et al. 2015a proposed the static and free vibration analyses of civil buildings and wing structures. Using the CW approach, various complex space structures have been proposed by Carrera et al. 2015c for the free vibration analysis of launchers. In the works of Carrera et al. 2016 and Petrolo et al. 2016, a new approach is used to model damaged aerospace structures, by changing the local stiffness getting various damage configurations in a simple manner. The free vibration analysis of aircraft structures was performed by Carrera and Zappino 2016. Inherently, Carrera et al. 2017 analyzed the effect of non-structural masses on the free vibration analysis of a launcher. Cavallo et al. 2018 included the effect of the composite materials for the dynamic analysis of space structures.

In the present paper, the CW approach is used to analyze the effect of damage on the free vibration analysis of different civil structures, with particular emphasis to truss structures, industrial buildings and a multi-floor building. The main novelty and advantage of the proposed CW methodology is that the modal analysis of typical civil engineering structures with component-wise, intra- and inter-component damages can be performed straightforwardly. In fact, because each components is modeled independently in this formulation and the governing equations of CUF, *per se*, are invariant of the theory approximation order, no ad-hoc techniques and mathematical artifices are needed in the construction of the model.

2 Refined one-dimensional models

The refined one-dimensional structural models used in the present work are based on the Carrera Unified Formulation. In the book of Carrera et al. 2014a, more details about beam, shell and solid FE models can be found. However, some details are outlined in the following for the sake of completeness.

2.1 Preliminary

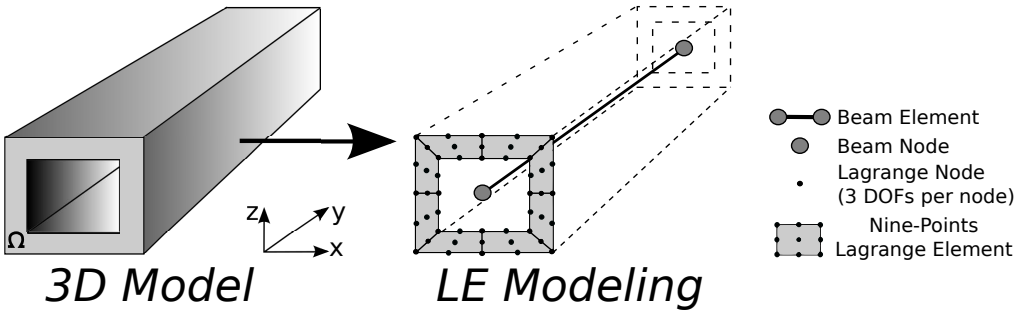

Figure 1: 1D-Refined model using the nine-points Lagrange elements.

Figure 1 shows the reference system used in the one-dimensional formulation, where the $y-axis$ is the beam axis, while the cross-section is identified by the x and $z-axes$. The symbol Ω stands the surface for the cross-section of the beam. The displacement vector can be written as:

$$\boldsymbol{u}(x,y,z) = \left\{ \begin{array}{ccc} u_x & u_y & u_z \end{array} \right\}^T \tag{1}$$

The three components u_x, u_y and u_z are the components of displacement vector $\boldsymbol{u}$ along the three directions x, y and z. The superscript T denotes transposition. Dependence on the time variable is omitted for simplicity purpose. The same form can be used for stress, σ, and strain, ϵ, vectors by using the following form:

$$\boldsymbol{\sigma} = \left\{ \begin{array}{cccccc} \sigma_{xx} & \sigma_{yy} & \sigma_{zz} & \sigma_{xy} & \sigma_{xz} & \sigma_{yz} \end{array} \right\}^T \tag{2}$$

$$\boldsymbol{\epsilon} = \left\{ \begin{array}{cccccc} \epsilon_{xx} & \epsilon_{yy} & \epsilon_{zz} & \epsilon_{xy} & \epsilon_{xz} & \epsilon_{yz} \end{array} \right\}^T \tag{3}$$

A linear model can be used to get the strain components from the displacement field:

$$\boldsymbol{\epsilon} = \mathbf{D}\boldsymbol{u} = \left([\mathbf{D}_y] + [\mathbf{D}_\Omega] \right) \boldsymbol{u} \tag{4}$$

$\mathbf{D}$ represents the differential operator and its explicit form can be found in Carrera et al. 2014a. $\mathbf{D}_y$ and $\mathbf{D}_\Omega$ are the differential operators on the beam axis y and over the beam cross-section, respectively. Concerning the constitutive relations, under the hypothesis of linear elastic materials materials, the Hooke's law can be written as:

$$\boldsymbol{\sigma} = \mathbf{C}\boldsymbol{\epsilon} \tag{5}$$

2.1.1 Lagrange-Like polynomials for the refined 1D model

The advantage of the CUF is that low- to higher-order kinematics for 1D beam theories can be formulated in an automatic and compact way by expressing the displacement field as an arbitrary expansion of the generalized displacement unknowns (see Carrera and Giunta 2010b, Carrera et al. 2014a):

$$\boldsymbol{u}(x, y, z) = F_\tau(x, z)\mathbf{u}_\tau(y) \tag{6}$$

where the index τ ranges from 1 to the number of terms used in the cross-sectional approximation. In this paper only the nine-point Lagrange Expansions (LE) are used, and they are:

$$\begin{gathered} F_\tau = \tfrac{1}{4}(r^2 + r\ r_\tau)(s^2 + s\ s_\tau) \qquad \tau = 1, 3, 5, 7 \\ F_\tau = \tfrac{1}{2}s_\tau^2(s^2 - s\ s_\tau)(1 - r^2) + \tfrac{1}{2}r_\tau^2(r^2 - r\ r_\tau)(1 - s^2) \qquad \tau = 2, 4, 6, 8 \\ F_\tau = (1 - r^2)(1 - s^2) \qquad \tau = 9 \end{gathered} \tag{7}$$

Where r and s range from -1 to $+1$. Figure 2 shows how the assembly of the LE polynomials over the

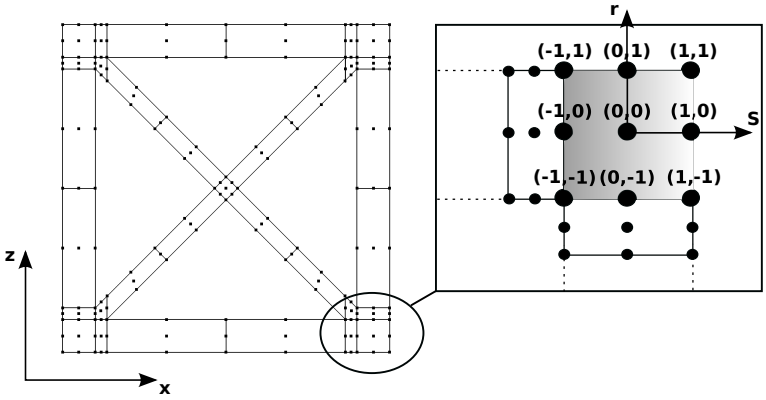

Figure 2: Cross-section discretization and assembly with the LE elements.

beam cross-section permits to describe a piece-wise refined kinematics able to deal with complex physics and geometries. More details on refined beam models can be found in the book by Carrera et al. 2011. In this work, nine-node Lagrange elements are mainly used to model each component. In fact, the accuracy of these models have been verified in several works, such as Cavallo et al. 2017.

2.1.2 Finite Element (FE) Solution

Along the $y - axis$ the generalized displacement vector, $u_\tau(y)$, can be approximated adopting the Finite Element Method (FEM) by using the classical beam shape functions. When a beam element with N_{NE} nodes along the axis is considered, the generalized displacement vector becomes:

$$\mathbf{u}_\tau(y) = N_i(y)\mathbf{q}_{i\tau}; \qquad i = 1 \dots N_{NE} \tag{8}$$

The index i ranges from 1 to the number of nodes per element N_{NE}. Therefore, the displacement field can assume the following form:

$$\mathbf{u}(x, y, z) = F_\tau(x, z)N_i(y)\mathbf{q}_{i\tau} \tag{9}$$

In Eq. (9) the index i stands for the node of the element along the y-axis. Three- ($B3$ element) and four-nodes ($B4$ element) refined beam elements are used in the present work.

2.2 Governing equations

The governing equations can be derived using the Principle of Virtual Displacements (PVD). According to dynamic case the PVD is:

$$\delta L_{int} = \delta L_{ext} - \delta L_{ine} \tag{10}$$

Where L_{int} stands for the internal work, L_{ext} is the external work due to the external loading, and L_{ine} stands the work of the inertial loadings. The virtual variation is expressed with the symbol δ. In the case of free vibration analysis, where the external loads are equal to zero, Eq. (10) becomes:

$$\delta L_{int} + \delta L_{ine} = 0 \tag{11}$$

The internal work can be written as following:

$$\delta L_{int} = \int_V \delta \boldsymbol{\epsilon}^T \boldsymbol{\sigma} dV \tag{12}$$

By using the constitutive equations (3) and the geometrical relations (2) and by adopting the displacement field form proposed in the equation (9), the variation of the internal work becomes:

$$\delta L_{int} = \delta \mathbf{q}_{\tau i}^T \int_V \left[\boldsymbol{D}^T (N_i(y) F_\tau(x,z)) \;\; \boldsymbol{C} \;\; \boldsymbol{D}(F_s(x,z) N_j(y)) \right] dV \mathbf{q}_{sj} = \delta \mathbf{q}_{sj}^T \boldsymbol{K}^{ij\tau s} \mathbf{q}_{\tau i} \tag{13}$$

The differential operator $\boldsymbol{D}$ works on F_τ, F_s, N_i and N_j. $\boldsymbol{K}^{ij\tau s}$ is the stiffness matrix expressed in form of "*fundamental nucleus*" and is a 3×3 array. $\mathbf{q}_{\tau i}$ is the vector of the nodal unknown and $\delta \mathbf{q}_{sj}$ is its virtual variation.

Similarly, for the work of the inertial loadings, the virtual variation becomes:

$$\delta L_{ine} = \int_V \delta \mathbf{u}^T \; \rho \; \ddot{\mathbf{u}} \;\; dV \tag{14}$$

where $\ddot{\mathbf{u}}$ is the acceleration vector and ρ stands the density of the material. Using Eq. (4), Eq. (14) can be rewritten as following:

$$\delta L_{ine} = \delta \mathbf{q}_{sj}^T \int_l N_i(y) \left\{ \int_\Omega \rho \left[F_\tau(x,z) \;\; F_s(x,z) \;\; \mathbf{I} \right] d\Omega \right\} N_j(y) dz \ddot{\mathbf{q}}_{\tau i} = \delta \mathbf{q}_{sj}^T \;\; \boldsymbol{M}^{ij\tau s} \;\; \ddot{\mathbf{q}}_{\tau i} \tag{15}$$

Where the mass matrix $\boldsymbol{M}^{ij\tau s}$ is a 3×3 *fundamental nucleus*. The explicit form of the fundamental nucleus for both the stiffness and the mass matrices can be found in Carrera et al. 2014a.

In conclusion, the final form of the equations of motion is:

$$\delta \mathbf{q}_{sj}^T \left(\boldsymbol{K}^{ij\tau s} \;\; \mathbf{q}_{\tau i} + \boldsymbol{M}^{ij\tau s} \;\; \ddot{\mathbf{q}}_{\tau i} \right) = 0 \tag{16}$$

The global stiffness and mass matrices are obtained using the classical FE assembling procedure, as shown in Carrera et al. 2014a. The equation for a free undamped problem can be written as:

$$\boldsymbol{M} \ddot{\mathbf{q}} + \boldsymbol{K} \mathbf{q} = 0 \tag{17}$$

Where $\mathbf{q}$ is the global unknowns vector. Due to linearity of the problem, according to harmonic solutions, the natural frequencies, ω_k, are obtained by solving the following eigenvalues problem:

$$\left(-{\omega_k}^2 \boldsymbol{M} + \boldsymbol{K} \right) \mathbf{q}_k = 0 \tag{18}$$

Where $\mathbf{q}_k$ is the *k-th* eigenvector, and k ranges form 1 to total numbers of DOF of the structures.

3 Numerical results

This section investigates the effect of various damaged components of the free vibration analysis of civil reinforced structures. In the damaged zone, the material characteristics are modified according to the formula proposed in the work of Carrera et al. 2016:

$$E_d = d \times E \qquad with \quad 0 \leq d \leq 1 \tag{19}$$

Three different levels of damage are considered in the present work. For a high damage level, d is equal to 0.8 with a reduction of E of 80 %; for moderate damage, d is assumed to equal to 0.5 halving the value of E; for small damage, a value of 0.2 is assigned to d. The notation used for the damaged structure concerns the use of an acronym composed of the letter D and a number for the damage, followed by a letter S, M or H for the intensity. To be specific, damage case 1 with d equal to 0.5 is called $D1^M$. The aforementioned damage scenarios are chosen for representative purposes to demonstrate the capability of the present approach to deal with damaged structures in a component-wise sense.

The structures considered are civil structures already established and assessed in Carrera et al. 2014b, where the results are compared to different Solid models studied using the commercial NASTRAN® code.

3.1 Truss

The first structure considered is a classical truss component. Figure 3 shows the whole geometry of the present reinforced model, and various information about the dimensions and the boundary conditions are highlighted. In particular, the dimensions are $a = b$ =0.2 [m], $t = a/10$, and $L = 10 \times a$. t is the dimension of the sides of the longitudinal and cross-sectional braces. Six hinged boundary conditions are applied on the external nodes, where the cross-section is reinforced with diagonal braces. The material used is a classical aluminium with a Young modulus, E, equal to 75 GPa, the Poisson ratio, ν, equal to 0.3 and the value of density, ρ, equal to 2700 $\frac{kg}{m^3}$.

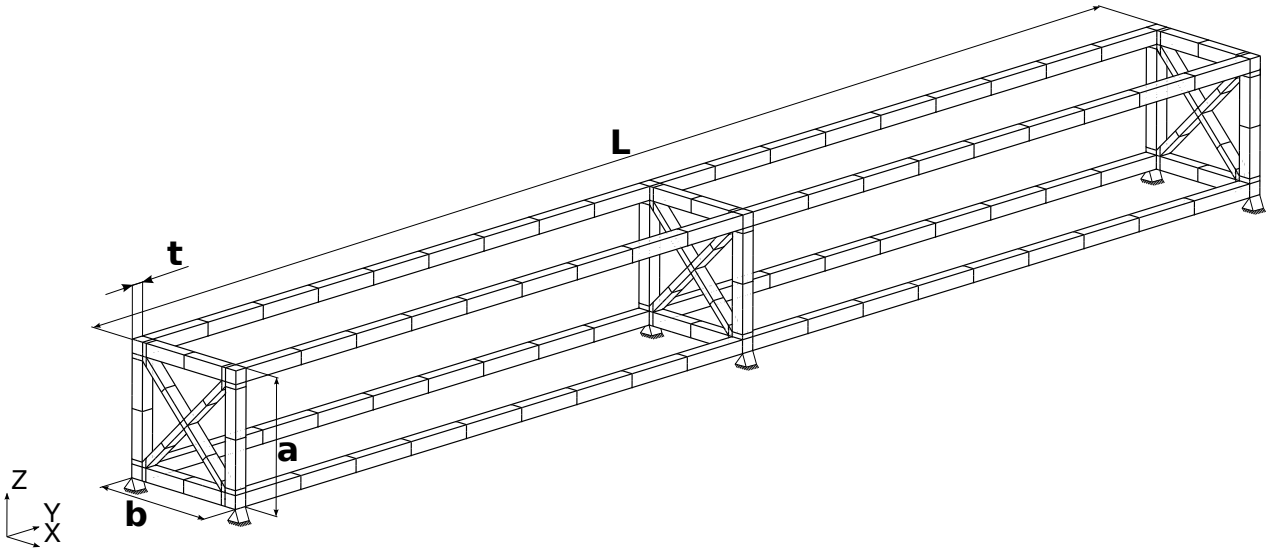

Figure 3: Truss structure.

Table 1 shows the results related to the first five frequencies between the undamaged structure (UND) and the solid model ($NAS3D$) from the commercial NASTRAN® code. The percentage different than the refined solid model ($NAS3D$) is less than 5% for all the frequencies considered. In addition, the UND DOFs are only 7% than the $NAS3D$ DOFs.

Model	NAS3D	UND
DOFs	98730	7308
Mode 1	88.1	$90.3^{(-2.5\%)}$
Mode 2	93.3	$96.4^{(+3.3\%)}$
Mode 3	96.2	$100.0^{(+3.9\%)}$
Mode 4	98.5	$103.8^{(+5.4\%)}$
Mode 5	101.3	$106.0^{(+4.6\%)}$

Table 1: The first five frequency of the truss structure by the present 1D approach and a 3D Nastran model.

The effect on the free vibration analysis of the different levels of damage is considered in this section. Three damage localized into various parts of the truss structure are taken into account including three intensities of damage represented by the letter S, M and H, as proposed in Figure 4 for *Damage* 1. The location of

damages 2 and 3 are proposed in Figure 5. For each damage case, the effect of damage intensity on the first 10 natural frequencies is further investigated in Figure6 and the results are shown in Table 2.

Mode 1 is firmly influenced by *Damage* 1, in fact for the medium and high level of intensity, D1$^{\text{M}}$ and D1$^{\text{H}}$, there is a sensible reduction of the first two natural frequencies, about 5.5%, and 15.5 %, respectively. In contrast *Damage* 2 does not produce a significant variation of mode 1 and 2. At the same way, the behavior of the first ten modes is almost constant considering damage 3, for all the damage intensities assumed.

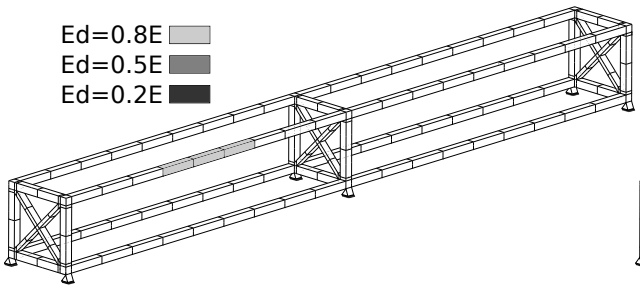

(a) *Small damage, D1*$^{\text{S}}$

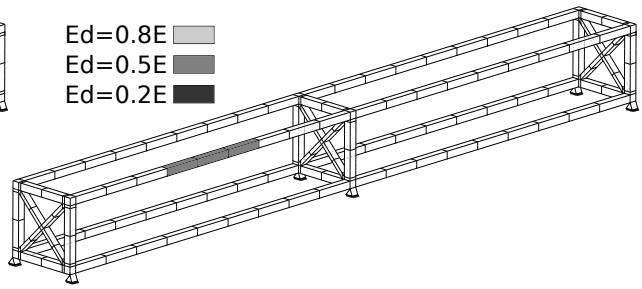

(b) *Intermediate damage, D1*$^{\text{M}}$

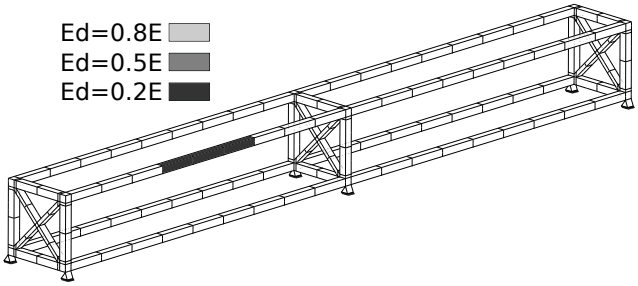

(c) *High damange, D1*$^{\text{H}}$

Figure 4: Truss structure affected by Damage 1 with different intensities.

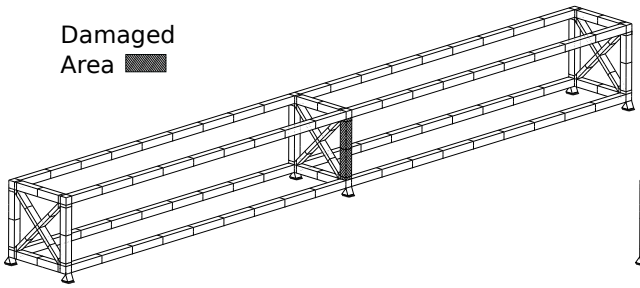

(a) *Location of Damage 2, D*2

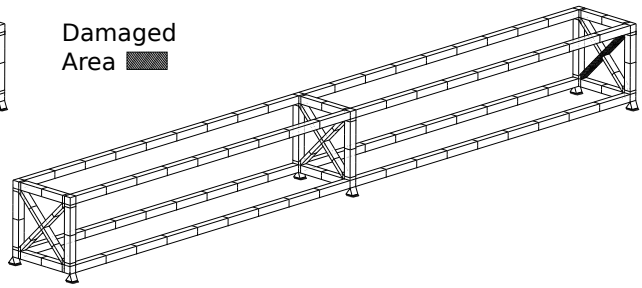

(b) *Location of Damage 3, D*3

Figure 5: Truss structure affected by Damages 2 and 3.

The Modal Assurance Criterion (MAC), see Allemang and Brown 1982, is used to compare the mode shapes between the undamaged and damaged configuration. The MAC is a scalar number that represents the degree of consistency between two vectors:

$$MAC_{ij} = \frac{\left|\{\phi_{A_i}\}^T\{\phi_{B_j}\}\right|^2}{\{\phi_{A_i}\}^T\{\phi_{A_i}\}\{\phi_{B_j}\}\{\phi_{B_j}\}^T} \tag{20}$$

where, $\{\phi_{A_i}\}$ is the i^{th}-eigenvector of model A, while $\{\phi_{B_j}\}$ is the j^{th}-eigenvector of model B. MAC ranges from zero, when two modes are completely different, to 1,when the maximum correspondence between two modes is achieved.

Figure 7 shows the MAC between the undamaged structure and the truss with $D1$ and different damage levels. Figures 7b and c highlight the high sensitivity of the structure when damage 1 is considered with

	Undamaged	Damage 1			Damage 2			Damage 3		
	Intensity	*S*	*M*	*H*	*S*	*M*	*H*	*S*	*M*	*H*
f_1	89.80	88.71	84.80	75.85	89.53	88.87	87.17	89.77	89.71	89.63
f_2	95.34	94.06	88.79	78.38	94.96	94.09	92.63	95.28	95.17	95.02
f_3	98.15	97.19	95.37	93.91	97.91	97.50	97.00	98.13	98.09	98.04
f_4	101.41	100.91	98.48	97.56	101.15	100.57	99.70	101.40	101.39	101.37
f_5	102.68	101.16	100.62	100.23	102.61	102.51	102.37	102.63	102.53	102.37
f_6	102.78	102.35	101.96	101.82	102.76	102.73	102.66	102.75	102.70	102.65
f_7	104.17	103.93	103.57	103.39	104.02	103.78	103.55	104.17	104.16	104.14
f_8	105.28	104.58	104.35	104.28	105.25	105.20	105.09	105.21	105.09	104.94
f_9	106.53	105.93	105.58	105.42	106.49	106.42	106.28	106.51	106.47	106.43
f_{10}	107.77	107.41	107.07	106.92	107.75	107.70	107.62	107.77	107.75	107.73
f_{11}	108.07	107.69	107.65	107.62	108.06	108.03	107.98	108.03	107.95	107.83
f_{12}	109.01	108.91	108.86	108.83	108.98	108.92	108.85	109.00	108.99	108.98
f_{13}	109.67	109.65	109.65	109.64	109.61	109.50	109.34	109.66	109.65	109.64
f_{14}	110.55	110.54	110.54	110.54	110.53	110.49	110.44	110.54	110.52	110.50
f_{15}	111.73	111.71	111.69	111.68	111.72	111.68	111.62	111.72	111.71	111.69

Table 2: First 15 natural frequencies in [Hz] of the truss structure for different damage cases.

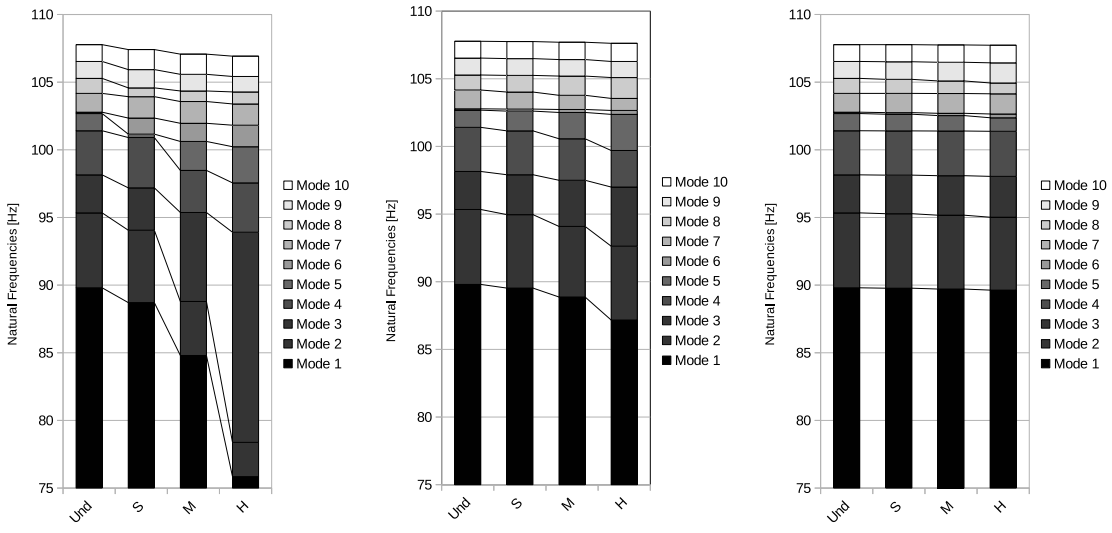

(a) *Damage 1* (b) *Damage 2* (c) *Damage 3*

Figure 6: Effect of damage intensity on the first ten natural frequencies of the truss structure.

high and medium damage intensities. In these cases, in fact, it is evident that the first three frequencies are also affected by the damage. In the case of $D1$ but with small intensity (see Figure 7a) and for all the other damages considered (Figures 8 and 9), the first three frequencies are not dependent on the damage.

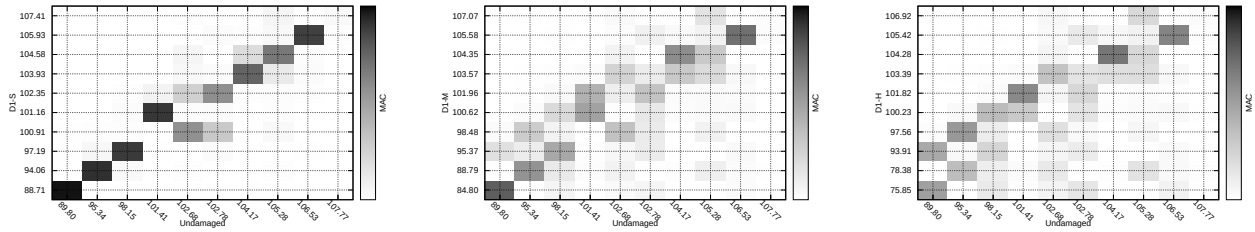

(a) *Damage* 1^S (b) *Damage* 1^M (c) *Damage* 1^H

Figure 7: MAC matrices of the truss structure affected by Damage 1 and different intensities.

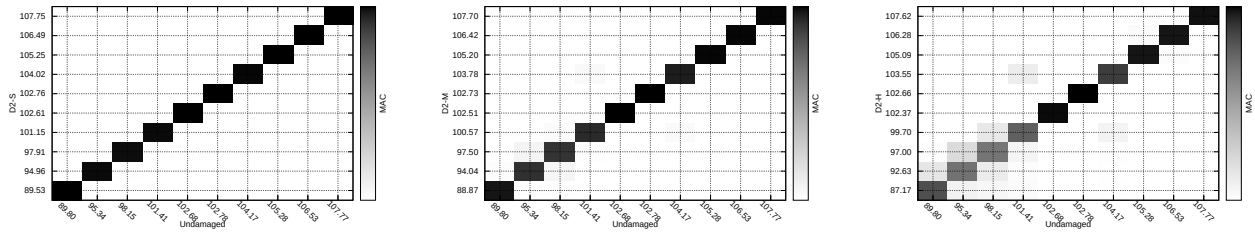

(a) *Damage* 2^S (b) *Damage* 2^M (c) *Damage* 2^H

Figure 8: MAC matrices of the truss structure affected by Damage 2 and different intensities.

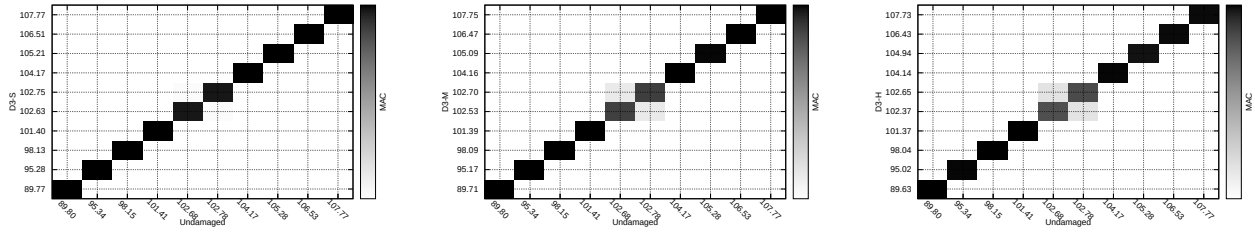

(a) *Damage* 3^S (b) *Damage* 3^M (c) *Damage* 3^H

Figure 9: MAC matrices of the truss structure affected by Damage 3 and different intensities.

Figure 10 highlights the ability of the present 1D-model to perform the free vibration analysis of complex civil reinforced structures subjected to damage. Figures 10b and c show the deformation of the longitudinal braces as mode 1 of the structure undamaged.

3.2 Industrial building

A classical industrial building is shown in Figure 11 where various information about the dimensions and the boundary conditions are included.

The geometrical dimensions are $L = 14.00$ [m], $b = 13.80$ [m], $c = 4.50$ [m], $a_1 = 7.00$ [m], $a_2 = 3.00$ [m]. Columns and frames have a square section with side 0.2 [m]. At the base of the columns, four clamped

(a) $f_1^{UND} = 89.80$ *[Hz]* (b) $f_1^{D1-H} = 75.85$ *[Hz]* (c) $f_3^{D1-H} = 93.91$ *[Hz]*

Figure 10: Mode shapes of the undamaged and damaged truss structure.

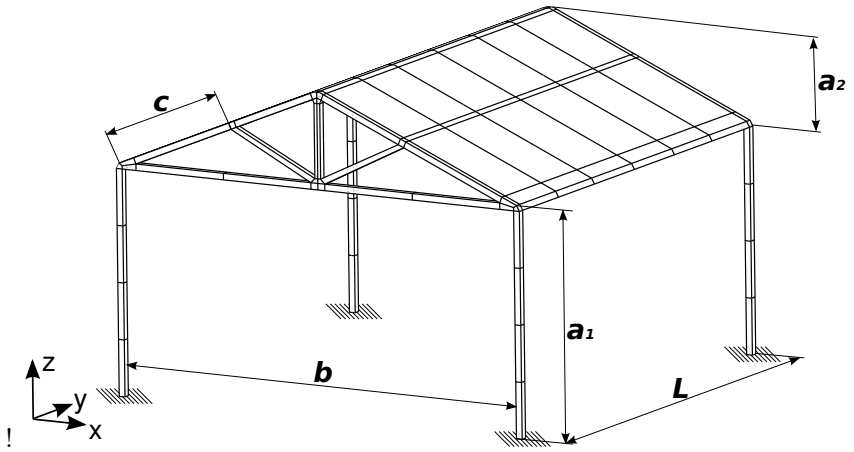

Figure 11: Industrial building.

boundary conditions are applied. For the sake of simplicity, the roof has the same thickness of the frame. All components are made using a unique metallic material characterized by a Young modulus, E, equal to 210 GPa, the Poisson ratio, ν, equal to 0.28 and the value of density, ρ, equal to 7850 $\frac{kg}{m^3}$.

Three different damage levels are of damage is considered,as in the previous analysis case. Figure 12 shows the areas where the damage is considered. Three are the components damaged in the whole structure, that is, a column, the central frame and a portion of the roof.

The following analyses are conducted considering each damage alone highlighting the effect of various levels of the damages considered on the first 15 frequencies in the case of free vibration analysis.

	Undamaged	Damage 1			Damage 2			Damage 3		
	Intensity	*S*	*M*	*H*	*S*	*M*	*H*	*S*	*M*	*H*
f_1	0.52	0.51	0.51	0.50	0.52	0.52	0.52	0.52	0.52	0.52
f_2	0.53	0.53	0.52	0.51	0.53	0.53	0.53	0.53	0.53	0.53
f_3	0.90	0.90	0.89	0.87	0.90	0.90	0.90	0.90	0.90	0.90
f_4	4.33	4.33	4.32	4.30	4.33	4.33	4.32	4.29	4.19	4.05
f_5	5.23	5.23	5.21	5.16	5.23	5.23	5.23	5.21	5.16	5.11
f_6	9.83	9.82	9.76	9.54	9.83	9.83	9.83	9.81	9.78	9.71
f_7	11.11	11.09	11.03	10.85	11.11	11.10	11.08	11.05	10.83	10.21
f_8	11.60	11.59	11.57	11.53	11.59	11.58	11.54	11.51	11.39	11.32
f_9	15.26	15.24	15.17	14.95	15.25	15.24	15.18	15.16	14.98	14.75
f_{10}	17.87	17.86	17.84	17.37	17.86	17.83	17.72	17.68	17.25	16.30
f_{11}	20.15	20.10	19.39	17.72	20.03	19.64	18.47	20.08	19.80	19.11
f_{12}	20.76	20.61	20.09	18.16	20.74	20.69	20.49	20.63	20.46	20.37
f_{13}	21.65	21.56	20.33	20.24	21.48	21.19	20.91	21.63	21.58	21.50
f_{14}	22.26	21.73	21.17	20.80	22.25	22.21	22.09	22.24	22.19	22.10
f_{15}	22.31	22.06	21.66	21.66	22.28	22.25	22.23	22.28	22.21	22.10

Table 3: First 15 natural frequencies in [Hz] of the industrial building for different damage cases and intensities.

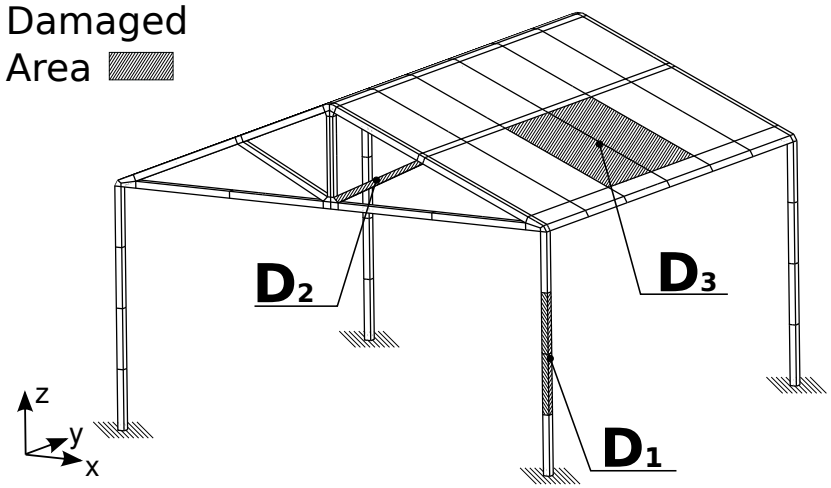

Figure 12: Damaged components of the industrial building.

Table 3 and Figure 13 show the natural frequencies behaviour for different damage scenarios. It is clear that the damages considered do not afflict the first ten frequencies as shown in the Figures 14, 15 and 16. When the roof is severely damaged, as shown in Figure16c, frequencies 7 and 8 suffer more than the other frequencies because these are the mode of the roof, as depicted in Figure 17.

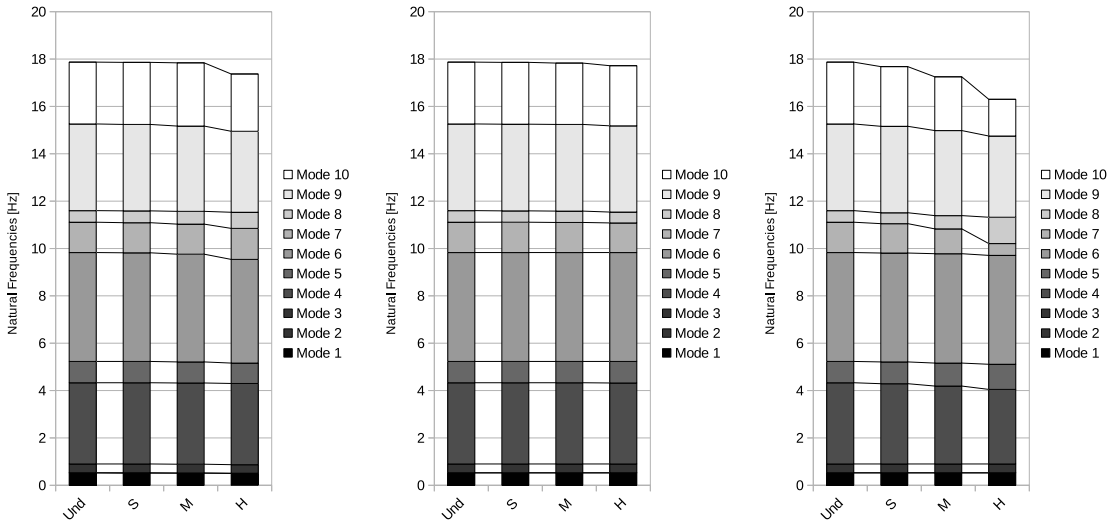

(a) *Damage 1* (b) *Damage 2* (c) *Damage 3*

Figure 13: Effect of damage intensity on the first ten natural frequencies of the industrial building.

3.3 Multi-floor building

The last structure considered is a simplified and a complete multi-floor building. The base of the building has a square shape, with three floors, one of which has a total length of 3 [m].

On the ground floor, there is a door, and the second and third floors have two windows along two sides, as shown in Figure18a. The four windows have the same dimensions, and they are equally located on both floors. The four columns are clamped on the ground to simulate the supporting structure. Two different materials are considered for the undamaged structure, in particular the columns are made of *Material 1* characterized by a Young modulus, E_1, equal to 210 GPa, the Poisson ratio, ν_1, equal to 0.28 and the value of density, ρ_1, equal to 7850 $\frac{kg}{m^3}$. The walls of the building are made of *Material 2* with E_2 equal to 48 GPa, ν_2 equal to 0.28 and ρ_2 is equal to 1570 $\frac{kg}{m^3}$. As in the previous case, three different intensity of damage are considered in three components, as shown in Figure18b. The levels of damage are applied to the Young modulus of the

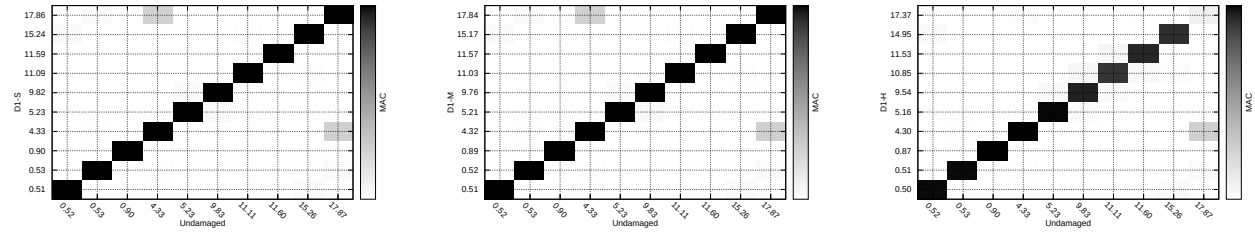

(a) *Damage* 1^S (b) *Damage* 1^M (c) *Damage* 1^H

Figure 14: MAC matrices of the industrial building affected by Damage 1 and different intensities.

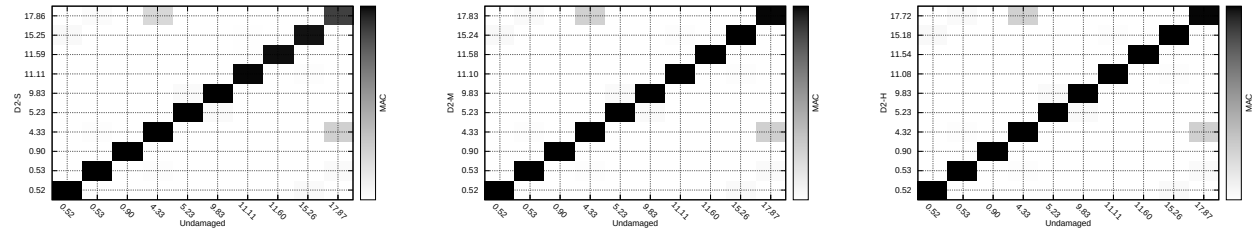

(a) *Damage* 2^S (b) *Damage* 2^M (c) *Damage* 2^H

Figure 15: MAC matrices of the industrial building affected by Damage 2 and different intensities.

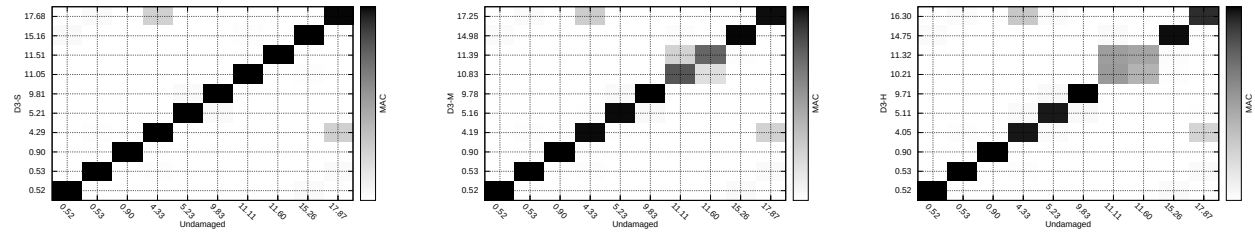

(a) *Damage* 3^S (b) *Damage* 3^M (c) *Damage* 3^H

Figure 16: MAC matrices of the industrial building affected by Damage 3 and different intensities.

(a) $f_7^{UND} = 11.11$ *[Hz]* (b) $f_8^{UND} = 11.60$ *[Hz]* (c) $f_7^{D3-H} = 10.21$ *[Hz]* (d) $f_8^{D3-H} = 11.32$ *[Hz]*

Figure 17: Representative mode shapes of the undamaged and damaged industrial building.

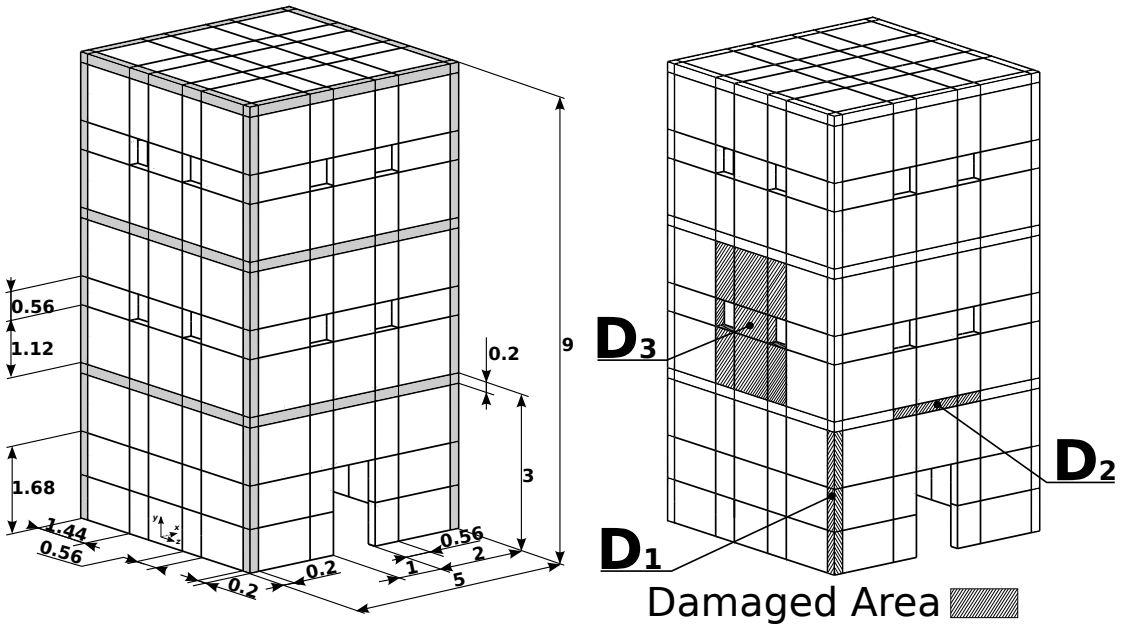

(a) *Geometrical properties expressed in meters* (b) *Damaged structure*

Figure 18: Dimensions of the multi-floor building and the damaged areas.

correspondent element, for example, if the damaged component is a column, the young modulus considered is E_1.

	Undamaged	Damage 1			Damage 2			Damage 3		
	Intensity	S	M	H	S	M	H	S	M	H
f_1	32.43	32.14	31.48	30.43	32.42	32.41	32.37	31.36	31.02	30.40
f_2	32.98	32.86	32.74	32.66	32.98	32.98	32.97	31.98	31.48	30.63
f_3	57.42	57.26	57.02	56.66	57.33	57.30	57.23	55.45	50.83	41.49
f_4	59.43	59.37	59.24	59.03	59.46	59.45	59.43	58.57	54.93	54.06
f_5	62.69	62.60	62.43	62.18	62.70	62.69	62.69	60.96	59.56	59.31
f_6	64.14	64.01	63.93	63.80	64.07	64.06	64.05	62.88	62.61	62.38
f_7	65.76	65.69	65.60	65.48	65.82	65.80	65.73	64.89	64.24	63.93
f_8	69.66	69.56	69.39	69.02	69.87	69.78	69.60	66.37	65.69	65.36
f_9	72.29	72.17	71.99	71.72	72.29	72.28	72.25	70.24	69.63	68.96
f_{10}	81.34	81.26	81.08	80.70	81.64	81.55	81.27	72.87	71.44	70.20
f_{11}	86.81	86.15	85.68	85.02	86.18	86.15	86.10	81.50	81.31	80.12
f_{12}	91.13	90.92	90.52	89.82	90.79	90.77	90.73	89.13	87.86	80.82
f_{13}	91.30	91.06	90.79	90.40	91.18	91.15	91.10	90.23	88.77	84.01
f_{14}	111.23	110.55	109.21	107.50	111.05	111.03	110.98	92.53	91.27	86.88
f_{15}	112.80	112.62	112.54	112.46	112.64	112.63	112.62	106.29	101.07	88.41

Table 4: First 15 natural frequencies in [Hz] of the multi-floor building for different damage cases and intensities.

The results in Table 4 show that the *Damage* 1 with small intensity does not afflict the first fifteen frequencies, and similarly this is confirmed in Figure 20a. For *Damage* 1 with higher intensity, the first two frequencies depend on the damage level, as depicted in Figures 20b and 20c. Figure 21 shows that the first fifteen frequencies do not depend on *Damage* 2. In contrast, the first four frequencies, with *Damage* 3^S, are not dependent on the defect introduced, but the other frequencies depend on the wall status. For a high level of *Damage* 3, the first frequencies modify the shape as proposed in Figure 23. The frequency 3 with *Damage* 3^M is not present as shown in Figure 22b, on the contrary the present mode appears in the undamaged structure.

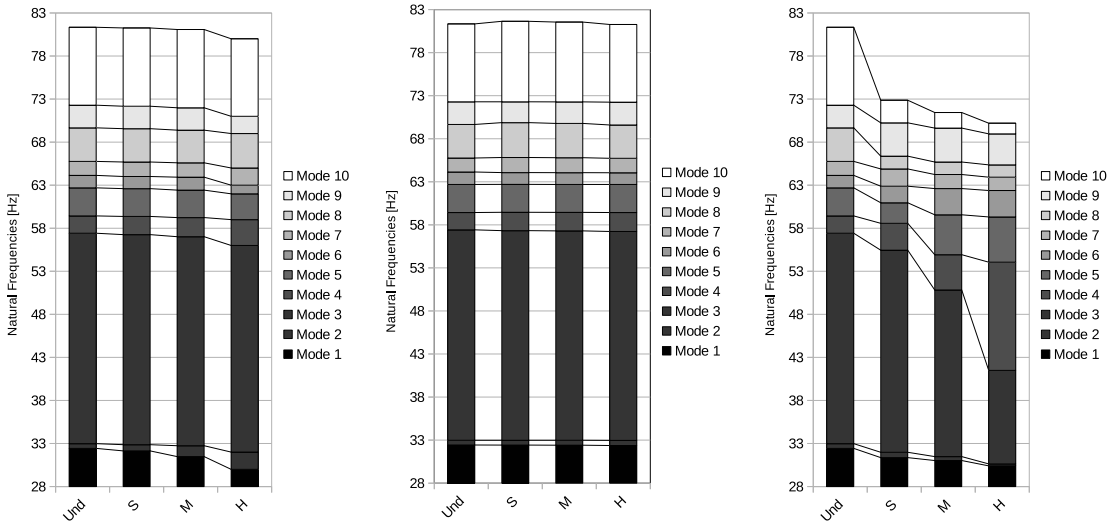

(a) *Damage 1* (b) *Damage 2* (c) *Damage 3*

Figure 19: Effect of damage intensity on the first ten natural frequencies of the multi-floor building.

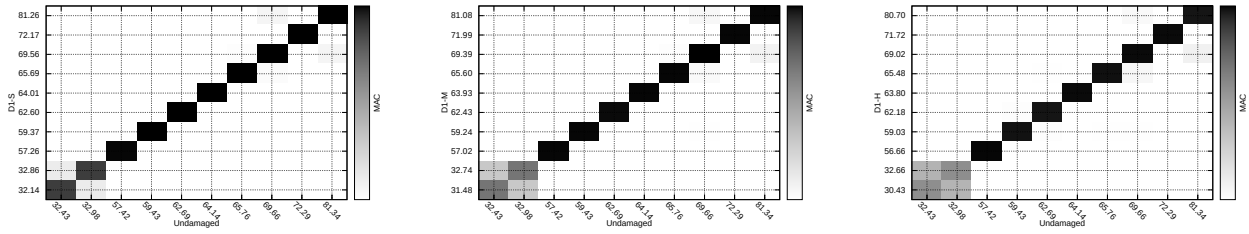

(a) *Damage* 1^S (b) *Damage* 1^M (c) *Damage* 1^H

Figure 20: MAC matrices of the multi-floor building affected by Damage 1 and different intensities.

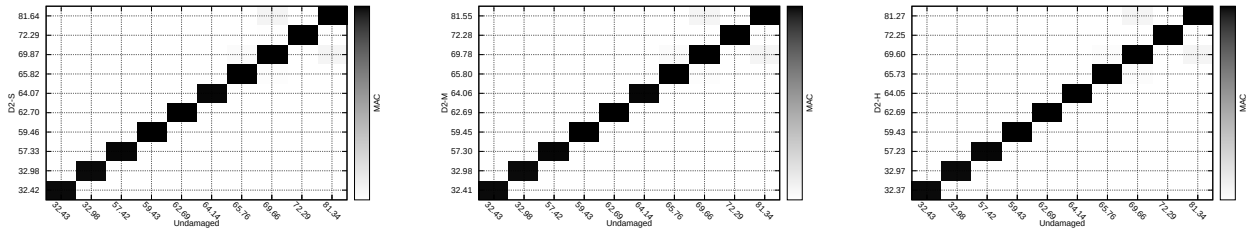

(a) *Damage* 2^S (b) *Damage* 2^M (c) *Damage* 2^H

Figure 21: MAC matrices of the multi-floor building affected by Damage 2 and different intensities.

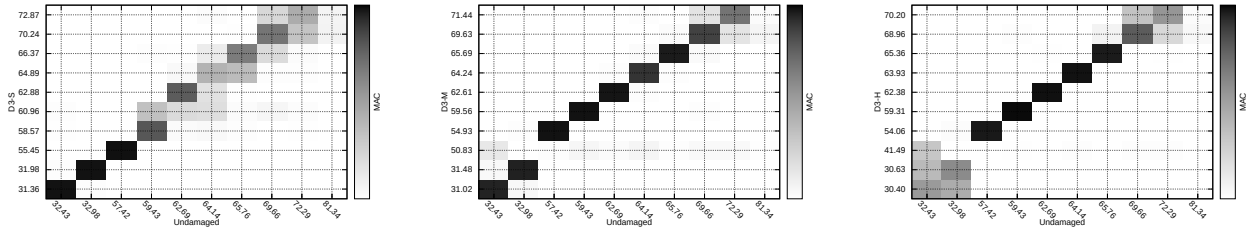

(a) *Damage* 3^S (b) *Damage* 3^M (c) *Damage* 3^H

Figure 22: MAC matrices of the multi-floor building affected by Damage 3 and different intensities.

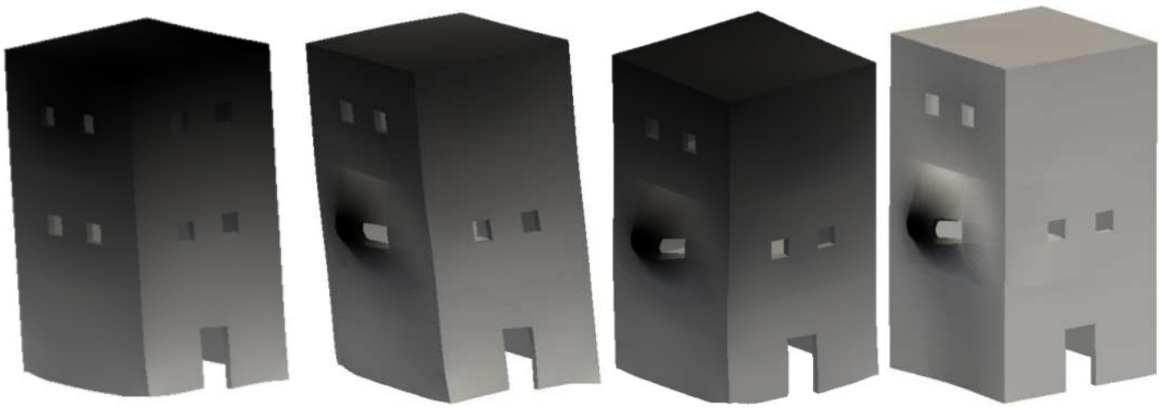

(a) $f_1^{UND} = 32.43$ *[Hz]* (b) $f_1^{D3-H} = 30.40$ *[Hz]* (c) $f_2^{D3-H} = 30.63$ *[Hz]* (d) $f_3^{D3-H} = 41.49$ *[Hz]*

Figure 23: Mode shapes of the undamaged and damaged multi-floor building.

4 Concluding Remarks

The present work has proposed advanced 1D models for the free vibration analysis of damaged civil structures, in particular, a truss component, an industrial structure and a multi-floor building. The analyses are carried out through a component-wise formulation based on CUF. The advantage of using Lagrange polynomials on the cross-section allows to the CW models to obtain complex multicomponent structures in an easy manner and with a high degree of accuracy. As such, CW models are particular interesting for the modelling of damaged structures. In fact, modern finite element methodologies can simulate damage and imperfections within the structure by penalization of single elements or groups of elements. As a consequence, the size of the mathematical model, i.e. the number of elements employed, is strictly related to the minimum dimensions of the damage. In other words, the finite element size may be as small as the minimum dimensions of the damage within the structure; thus, computational costs can increase considerably as analysts are interested in the simulation of structures affected by small damages. On the other hand, the present CW model can simulate multi-component, possibly in a multi-scale framework, within the single finite element. In this manner, the mesh is completely independent of the damage size and intensity.

Many other conclusions can be extrapolated from the analysis of the proposed results:

- the refined 1D models allow to analyse complex civil structures like the 3D models overcoming the limits of the classical one-dimensional models;
- the computational costs can be reduced using the CW approach including an accurate analysis of damaged structure;
- the analyzed sectional distorsion, using beam models, is worsened by local damage;
- the intensity and the position of the damage affect frequencies and mode shapes;

In conclusion, the refined CUF models are very attractive for the analysis of damaged structure. Extension to more complex cases, as well as multiple damages in civil and aerospace structures, could be a significant extension of the proposed investigation. Moreover, future analyses could be focussed the simulation of structures affected by low levels of damage intensities in order to assess the sensitivity of vibration-based methodologies for damage detection.

References

R. J. Allemang and D. L. Brown. A correlation coefficient for modal vector analysis. *Proceedings of the 1st SEM International Modal Analysis Conference*, pages 110–116, 1982. Orlando, FL, November 8-10.

V. L. Berdichevsky, E. Armanios, and A. Badir. Theory of anisotropic thin-walled closed-cross-section beams. *Composites Eng.*, 2(5-7):411–432, 1992.

R. Capozucca. Vibration of cfrp cantilever beam with damage. *Composite Structures*, 116:211222, 2014.

E. Carrera. A class of two dimensional theories for multilayered plates analysis. *Atti Accademia delle Scienze di Torino, Memorie Scienze Fisiche*, 19-20:49–87, 1995.

E. Carrera. Theories and finite elements for multilayered, anisotropic, composite plates and shells. *Archives of Computational Methods in Engineering*, 9(2):87–140, 2002.

E. Carrera. Theories and finite elements for multilayered plates and shells: a unified compact formulation with numerical assessment and benchmarking. *Archives of Computational Methods in Engineering*, 10(3): 216–296, 2003.

E. Carrera and G. Giunta. Refined beam theories based on a unified formulation. *Int. J. Appl. Mech.*, 2(1): 117–143, 2010a.

E. Carrera and G. Giunta. Refined beam theories based on a unified formulation. *International Journal of Applied Mechanics*, 2(1):117–143, 2010b.

E. Carrera and E. Zappino. Carrera unified formulation for free-vibration analysis of aircraft structures. *AIAA Journal*, 54(1):280–292, 2016.

E. Carrera, G. Giunta, and Petrolo M. *Beam Structures, Classical and Advanced Theories.* John Wiley & Sons, 2011.

E. Carrera, A. Pagani, and M. Petrolo. Classical, refined, and component-wise analysis of reinforced-shell wing structures. *AIAA*, 51(5), 5 2013a. DOI: 10.2514/1.J052331.

E. Carrera, A. Pagani, and M. Petrolo. Component-wise method applied to vibration of wing structures. *Journal of Applied Mechanics*, 88(4):041012–1–041012–15, 2013b.

E. Carrera, M. Cinefra, M. Petrolo, and E. Zappino. *Finite Element Analysis of Structures Through Unified Formulation.* John Wiley & Sons, 2014a.

E. Carrera, A. Pagani, and M. Petrolo. Free vibration analysis of civil engineering structures by component-wise models. *Journal of sound and vibration*, 333:4597–4620, 2014b.

E. Carrera, A. Pagani, and M. Petrolo. Refined 1d finite elements for the analysis of secondary, primary, and complete civil engineering structures. *Journal of Structural Engineering ASCE*, 141(4), 2015a. art. no. 04014123, doi: 10.1061/(ASCE)ST.1943-541X.0001076.

E. Carrera, A. Pagani, M. Petrolo, and E. Zappino. Recent developments on refined theories for beams with applications. *Mechanical Engineering Reviews, Bulletin of the Japan Society of Mechanical Engineers JSME*, 2(2):14–00298, 2015b.

E. Carrera, E. Zappino, and T. Cavallo. Accurate free vibration analysis of launcher structures using refined 1d models. *International Journal of Aeronautical and Space Sciences (IJASS)*, 16(2):206–222, 2015c.

E. Carrera, A. Pagani, and M. Petrolo. Free vibration of damaged aircraft structures by component-wise analysis. *AIAA Journal*, 54(10):3091–3106, 2016.

E. Carrera, E. Zappino, and T. Cavallo. Effect of solid mass consumption on the free-vibration analysis of launchers. *Journal of Spacecraft and Rockets (AIAA)*, 54(3):773–780, 2017.

T. Cavallo, E. Zappino, and E. Carrera. Component-wise vibration analysis of stiffened plates accounting for stiffener modes. *CEAS Aeronautical journal*, 8(2):385–412, 2017.

T. Cavallo, E. Zappino, and E. Carrera. Free vibration analysis of space vehicle structures made by composite materials. *Composite structures*, 183:53–62, 2018.

S. Doebling and C. R. Farrar. Using statistical analysis to enhance modal-based damage identification. in structural damage assessment using advanced signal processing procedures. *Sheffield Academic Press*, pages 199–212, 1997. Editors, Dulieu, J. M. and Staszewski, W. J. and Worden, K.

R. El Fatmi. Nonuniform warping including the effects of torsion and shear forces. part i: A general beam theory. *Int. J. Solids Struct.*, 44(18-19):5912–5929, 2007a.

L. Euler. De curvis elasticis. methodus inveniendi lineas curvas maximi minimive proprietate gaudentes, sive solutio problematis iso-perimetrici lattissimo sensu accepti. 1744. Bousquet, Geneva.

R. K. Kapania and S. Raciti. Recent advances in analysis of laminated beams and plates, part i: shear effects and buckling. *AIAA Journal*, 27(7):923–935, 1989a.

R. K. Kapania and S. Raciti. Recent advances in analysis of laminated beams and plates, part ii: vibrations and wave propagation. *AIAA Journal*, 27(7):935–946, 1989b.

A. S. Kiremidjian, E. G. Straser, T. Meng, K. Law, and H. Sohn. Structural damage monitornig for civil structures. *Structural Health Monitoring Current Status and Perspectives*, pages 371–382, 1997.

Kennedy D. Labib, A. and C. Featherston. Free vibration analysis of beams and frames with multiple cracks for damage detection. *Journal of Sound and Vibration*, 333(20):4991–5003, 2014.

K. Nguyen. Mode shapes analysis of a cracked beam and its application for crack detection. *Journal of Sound and Vibration*, 333(3):848–872, 2014.

M. Pérez, L. Gil, M. Snchez, and S. Oller. Comparative experimental analysis of the effect caused by artificial and real induced damage in composite laminates. *Composite Structures*, 112:169178, 2014.

M Petrolo, E. Carrera, and A. S. A. S. Alawami. Free vibration analysis of damaged beams via refined models. *Advances in Aircraft and Spacecraft Science*, 3(1), 2016. 95-112.

M. Pirner and O. Fisher. Monitoring stress in the grp extension of the prague tv tower. in structural damage assessment using advanced signal processing procedures. *Sheffield Academic Press*, pages 451–460, 1997. Editors, Dulieu, J. M. and Staszewski, W. J. and Worden, K.

H. Pollayi and W. Yu. Modeling matrix cracking in composite rotor blades within vabs framework. *Composite Structures*, 110:6276, 2014.

R. Schardt. Verallgemeinerte technische biegetheorie. *Springer-Verlag*, 1989. Berlin.

N. Silvestre and D. Camotim. First-order generalised beam theory for arbitrary orthotropic materials. *Thin-Walled Struct.*, 40(9):791–820, 2002.

I. S. Sokolnikoff. Mathematical theory of elasticity. *McGraw-Hill*, 1956. New York.

S. P. Timoshenko and J. N. Goodier. Theory of elasticity. *McGraw-Hill.*, 1970.

Y. Wang, M. Liang, and J. Xiang. Damage detection method for wind turbine blades based on dynamics analysis and mode shape difference curvature information. *Mechanical Systems and Signal Processing*, 48: 351367, 2014.

X. Wu, J. Ghaboussi, and J.H. Garrett. Use of neutral networks in detection of structural damage. *Computers and Structures*, 42(4):649–659, 1992.

W. Yu, V. V. Volovoi, D. H. Hodges, and X. Hong. Validation of the variational asymptotic beam sectional analysis. *AIAA Journal*, 40(10):21052112, 2002.

Z. Zhang, K. Shankar, E. Morozov, and M. Tahtali. Vibration-based delamination detection in composite beams through frequency changes. *Journal of Vibration and Control*, 22(2):496–512, 2016.

List of Figures